Computer Methods and Programs in Biomedicine 231 (2023) 107417

Contents lists available at ScienceDirect

Computer Methods and Programs in Biomedicine

journal homepage: www.elsevier.com/locate/cmpb

MRI-based mechanical analysis of carotid atherosclerotic plaque using a material-property-mapping approach
A material-property-mapping method for plaque stress analysis

Jessica Benitez Mendieta[a], Davide Fontanarosa[b], Jiaqiu Wang[a], Phani Kumari Paritala[a], Juanita Muller[d], Thomas Lloyd[e], Zhiyong Li[a,c,*]

[a] School of Mechanical, Medical and Process Engineering, Queensland University of Technology, Brisbane 4000, Australia
[b] School of Clinical Sciences, Queensland University of Technology, Brisbane 4000, Australia
[c] Faculty of Sports Science, Ningbo University, Ningbo 315211, China
[d] Department of Vascular Surgery, Princess Alexandra Hospital, Brisbane 4102, Australia
[e] Department of Radiology, Princess Alexandra Hospital, Brisbane 4102, Australia

ARTICLE INFO

Article history:
Received 7 November 2022
Revised 23 January 2023
Accepted 7 February 2023

Keywords:
Carotid stenosis
Mechanical analysis
Computational fluid dynamics
Mesh
Material properties

ABSTRACT

Background and objective: Atherosclerosis is a major underlying cause of cardiovascular conditions. In order to understand the biomechanics involved in the generation and rupture of atherosclerotic plaques, numerical analysis methods have been widely used. However, several factors limit the practical use of this information in a clinical setting. One of the key challenges in finite element analysis (FEA) is the reconstruction of the structure and the generation of a mesh. The complexity of the shapes associated with carotid plaques, including multiple components, makes the generation of meshes for biomechanical computation a difficult and in some cases, an impossible task. To address these challenges, in this study, we propose a novel material-property-mapping method for carotid atherosclerotic plaque stress analysis that aims to simplify the process.

Methods: The different carotid plaque components were identified and segmented using magnetic resonance imaging (MRI). For the mapping method, this information was used in conjunction with an in-house code, which provided the coordinates for each pixel/voxel and tissue type within a predetermined region of interest. These coordinates were utilized to assign specific material properties to each element in the volume mesh which provides a region of transition. The proposed method was subsequently compared to the traditional method, which involves creating a composed mesh for the arterial wall and plaque components, based on its location and size.

Results: The comparison between the proposed material-property-mapping method and the traditional method was performed in 2D, 3D structural-only, and fluid-structure interaction (FSI) simulations in terms of stress, wall shear stress (WSS), time-averaged WSS (TAWSS), and oscillatory shear index (OSI). The stress contours from both methods were found to be similar, although the proposed method tended to produce lower local maximum stress values. The WSS contours were also in agreement between the two methods. The velocity contours generated by the proposed method were verified against phase-contrast magnetic resonance imaging (MRI) measurements, for a higher level of confidence.

Conclusion: This study shows that a material-property-mapping method can effectively be used for analyzing the biomechanics of carotid plaques in a patient-specific manner. This approach has the potential to streamline the process of creating volume meshes for complex biological structures, such as carotid plaques, and to provide a more efficient and less labor-intensive method.

Abbreviations: CVD, Cardiovascular Diseases; FEA, Finite Element Analysis; CFD, Computational Fluid Dynamics; FSI, Fluid Structure Interaction; WSS, Wall Shear Stress.

* Corresponding author at: School of Mechanical, Medical, and Process Engineering, Queensland University of Technology (QUT), 2 George St, Brisbane, QLD 4000, Australia.
E-mail address: zhiyong.li@qut.edu.au (Z. Li).

https://doi.org/10.1016/j.cmpb.2023.107417

1. Introduction

Atherosclerosis is a major underlying cause of cardiovascular diseases (CVD) and is one of the leading causes of heart attacks, strokes, and other peripheral vascular complications. It is characterized by the narrowing and thickening of the arteries due to the accumulation of cholesterol and other lipids in the inner layer of the artery [1]. The rupture of atherosclerotic plaques located in the carotid artery is a major cause of most cerebral ischemic attacks [2,3]. Additionally, the rupture of an atherosclerotic plaque is fundamentally a mechanical event in which the stress levels exceed the strength of the tissue [4,5].

Advances in medical imaging, computational modeling, and simulation have greatly improved our understanding of plaque progression and rupture. These simulations include structural finite element analysis (FEA) [6,7], computational fluid dynamics (CFD) [8–10], and fluid-structure interaction (FSI). These methods allow for the detailed analysis of flow patterns, stress, and strain distributions that would otherwise not be possible to acquire from experimental or clinical imaging analysis.

While significant progress has been made in understanding the biomechanics of carotid artery disease through the use of finite element analysis (FEA) simulations, there is still a need for faster and simpler methods that can be translated to the clinical setting. Current methods are often hindered by the complexity of generating volume meshes, making it difficult to analyze a large cohort of patients. Traditional methods of mesh generation rely on creating a mesh for each individual plaque component and surrounding structures [6,11,12]. However, this approach is not suitable for complex shapes or multi-component models. Furthermore, in some instances, achieving a reasonable mesh requires further modification of the geometries, especially at the interfaces of the plaque components.

Another approach, known as the component fitting mesh generation technique, tries to address these issues by adding a number of lines to the models to generate smaller subvolumes, reducing the complexity of the model to facilitate meshing generation [13]. However, this is a simple approach that is labor-intensive, as the modeller has to perform the process slice by slice. Therefore, there is a need for a simplified meshing method for structural analysis of carotid plaque geometries that can be used with ease on MRI data from a large cohort of patients.

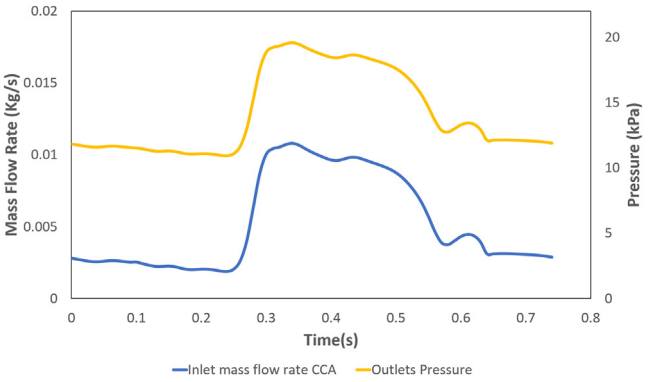

Fig. 1. Pressure profile (yellow line) applied at the internal wall for 2D and 3D structural-only simulations, and as outlets at the ICA and ECA for fluid-structure interaction (FSI) simulations. The mass flow rate profile (blue line) is prescribed as an inlet at the CCA for FSI simulations.

In this study, a method was developed to apply material properties to complex geometries such as carotid atherosclerotic plaques, including its components, by using isotropic material properties as a starting point and as a proof of concept. With this method, multi-component plaques can be evaluated without relying on meshing every single component, instead, the material properties were assigned to each element of a volume mesh. This process was achieved by developing a code that obtains the coordinates and tissue type for each pixel/voxel in the segmented images from magnetic resonance imaging (MRI).

The results of the traditional method and the new material-property-mapping method were compared in terms of principal stress in 2D, 3D structural, and fluid-structure interaction simulations. Additionally, the wall shear stress (WSS) contours at peak systole and diastole, time-averaged WSS (TAWSS), and oscillatory shear index (OSI) calculated from the FSI models were also compared. To identify the regions with the highest differences between both methods, the calculated stress and WSS values were subtracted. The results showed that the material-property-mapping method (from now on referred to as the mapping method) presents a faster and simpler approach for the assignment of material properties on atherosclerotic plaque geometries for subsequent computational simulation.

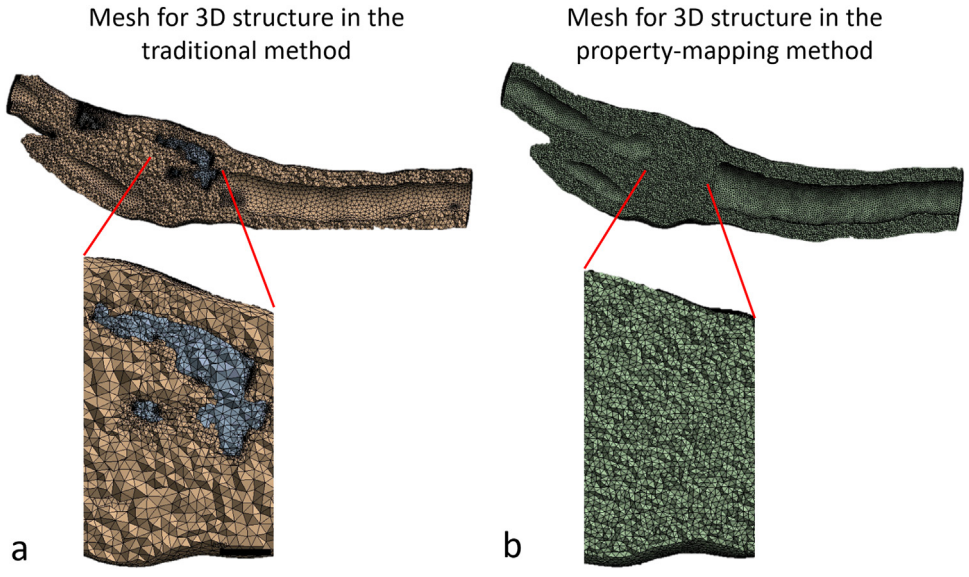

Fig. 2. Generated mesh using the (a) Traditional method and (b) material-property-mapping method for the analyzed blood vessel.

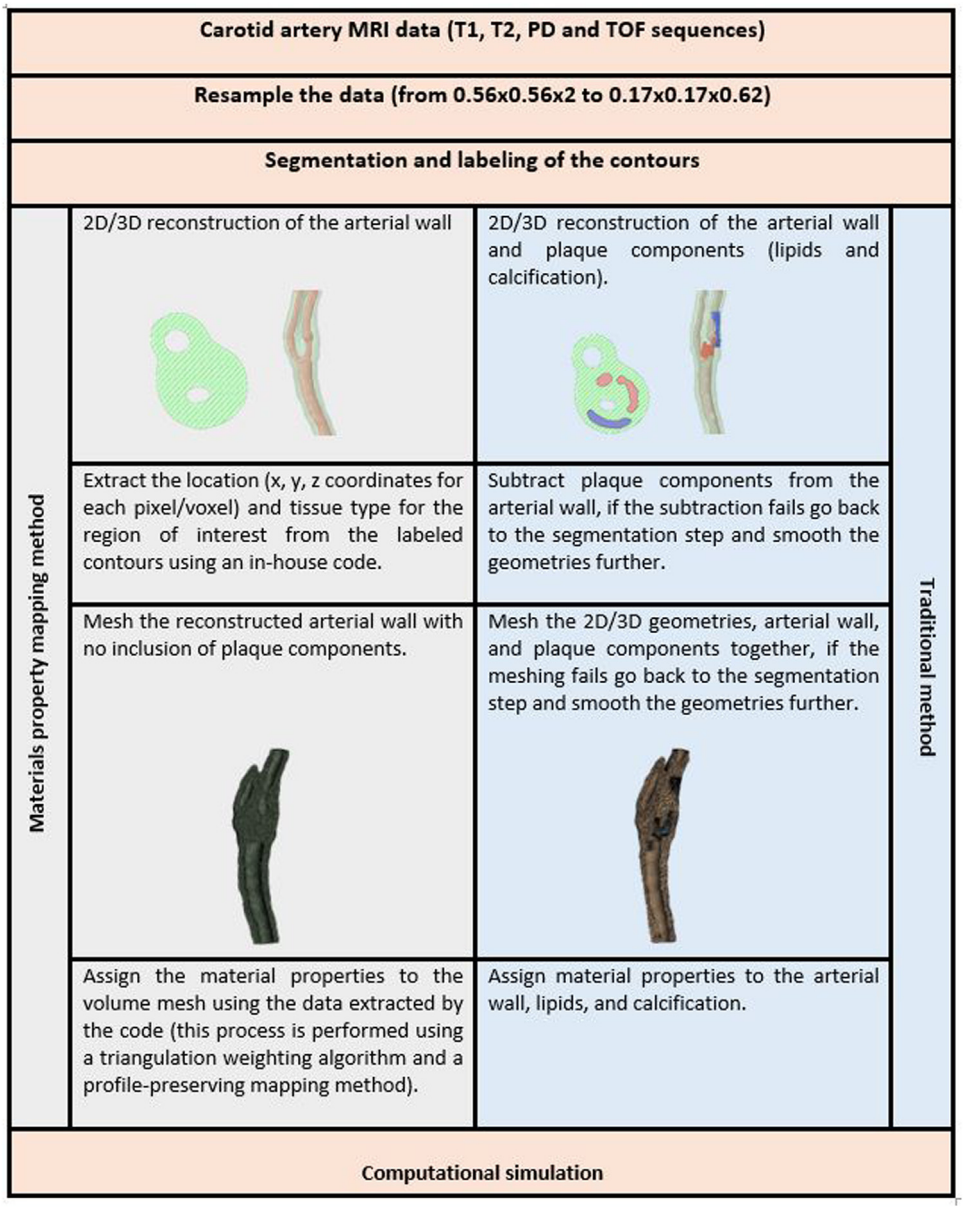

Fig. 3. Diagram of the different steps comparing the traditional and the material-property-mapping methods. The common steps shared by both methods are represented in pink, while the specific steps for the material-property-mapping method are represented in gray and the specific steps for the traditional method are represented in blue. This diagram shows the distinctions between the two methods and highlights the unique steps involved in each approach.

2. Materials and methods

2.1. MRI, segmentation, and boundary conditions

In this study, one patient with identified carotid stenosis (>90% based on Ultrasound (US) doppler) was scanned using MRI before carotid endarterectomy (CEA). Written consent was obtained from the patient (gender=female, age=77, current smoker, BMI=16), and detailed information about MRI protocol is provided in the supplementary material.

The 2D segmentation was performed using ImageJ (imagej.nih.gov/ij/) and the point coordinate tool. For the 3D reconstruction, our established protocol [10,14,15] was used to segment the patient-specific geometry. In brief, to describe the method, T1-weighted (T1) scans were employed to identify plaque components such as lipids, calcification, and arterial wall using Amira software (version 6.0, FEI, Hillsboro, Oregon, USA). T2-weighted (T2), proton-density weighted (PD), and time of flight (TOF) sequences were also utilised for plaque component identification.

Mass flow rate was extracted from phase-contrast MRI (PC-MRI) which also was employed in FSI analysis as inlet at the common carotid artery (CCA). The pressure applied to the internal region in the 2D and 3D structural-only analysis was calculated using the patient-specific arm-pressure scaled based on the mass flow rate profile. For FSI analysis this pressure was utilised as outlets at the internal carotid artery (ICA) and external carotid artery (ECA) (Fig. 1).

2.2. Traditional 2D, 3D structural, and FSI method

The reconstructed 2D surfaces were converted to solids in the design modeller software of ANSYS Workbench (version 19.0, ANSYS, Canonsburg, PA, USA). Boolean operations were used to subtract the solids of calcification and lipids from the arterial wall for

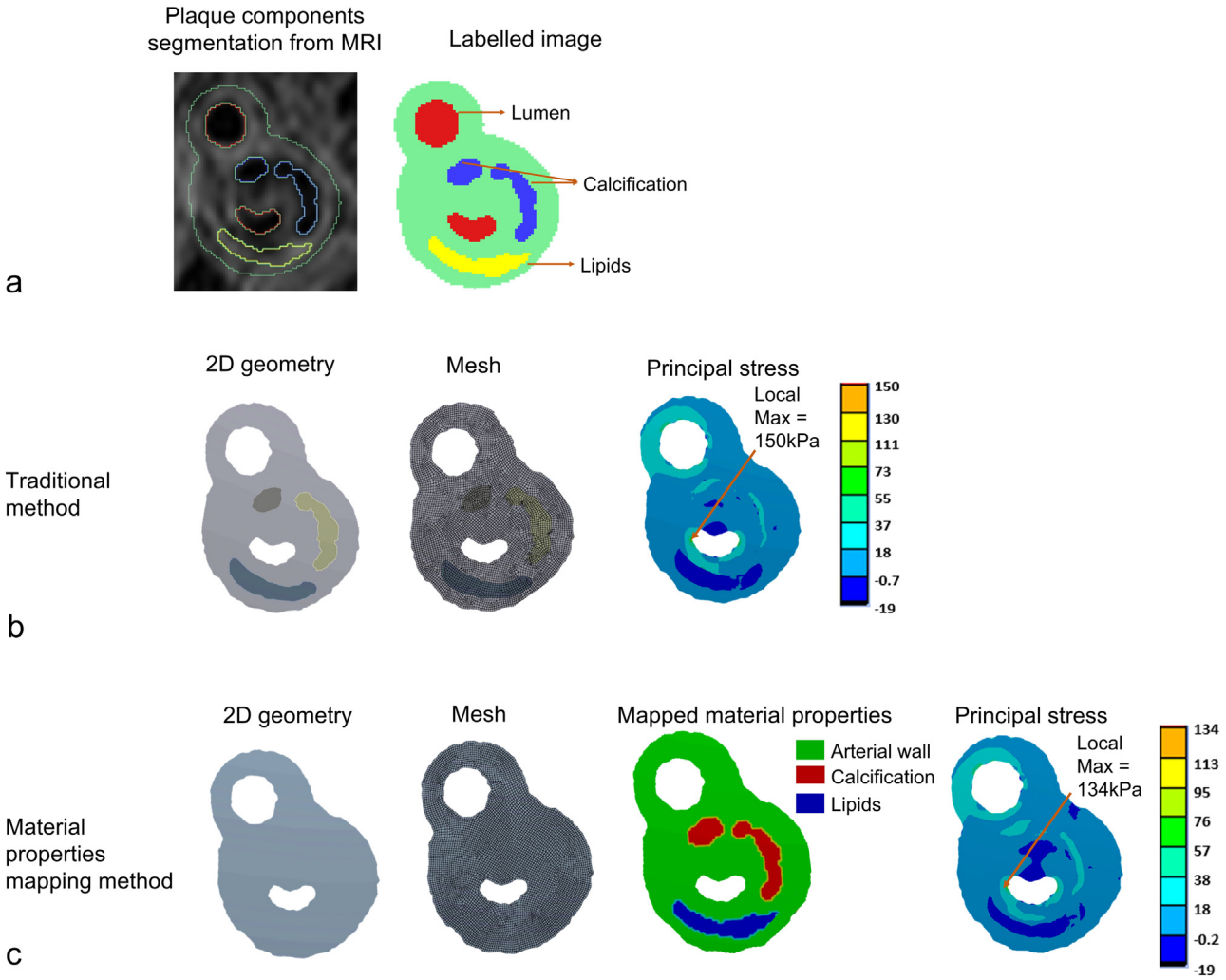

Fig. 4. (a) Example of a segmented MRI slice and the respective label (b) 2D geometry, mesh, and principal stress contour calculated using the traditional method. (c) 2D geometry, mesh, mapped material properties, and principal stress contour calculated using the material-property-mapping method.

both 2D and 3D structural analyses and fluid-structure interaction (FSI) in ANSYS SpaceClaim (version 19.0, ANSYS, Canonsburg, PA, USA). The entire structure, including multiple plaque components, was meshed using a curvature and proximity function (Fig. 2(a)). For the 2D and 3D structural analyses, the pressure was applied to the internal wall of the structure, while for FSI, the inner surface was set as a fluid-solid data transfer point. The only force applied in FSI was the transferred pressure between the fluid and structure (two-way FSI). Additional information about FSI settings is provided in the supplementary material.

A fixed (3D) and elastic (2D) support were also applied to the structures. The material properties for the vessel wall and plaque components were assumed to be isotropic elastic, with Poisson's ratio of 0.48 for all materials, and Young's Modulus of 10 MPa for calcification, 0.02 MPa for lipids, and 0.6 MPa for arterial tissue [16–20]. Linear material properties were applied to the plaque components due to the small deformation observed in the stenotic artery [14].

2.3. Mapping material properties in 2D, 3D structural, and FSI method

The mapping method required two types of data from MRI: the structure of the arterial wall without lumen or components and labels of the segmented plaque components within the wall. Then, the reconstructed geometry of the arterial wall was converted to solid and meshed to obtain a uniform mesh (Fig. 2(b)) with an element size of 0.3 mm. Material properties were then mapped using the labels and an in-house code developed in Matlab (R2018a, MathWorks, Natick, MA, USA). In the code, the labels were imported, and a region of interest was selected that corresponds to the atherosclerotic plaque to be studied. The code provided the coordinates (X, Y, and Z information) for each pixel/voxel and their respective tissue type. The results from the code were imported into the solver and each tissue type was assigned a specific Young's modulus (calcification (10 MPa), lipids (0.02 MPa), and the arterial wall (0.6 MPa)) and Poisson's ratio (0.48 for all materials). Each element in the mesh was then mapped with a corresponding material property using the information generated by the code and an external data system in the solver. The boundary conditions and fixed support were the same as those in the traditional method. Figure 3 provides a comparison between the traditional and the material property mapping method. Further information about settings and functions used in the mapping method is given in the supplementary material.

2.4. Solution methods

For this study one patient with carotid atherosclerosis was selected; this specific plaque had the inclusion of calcification and

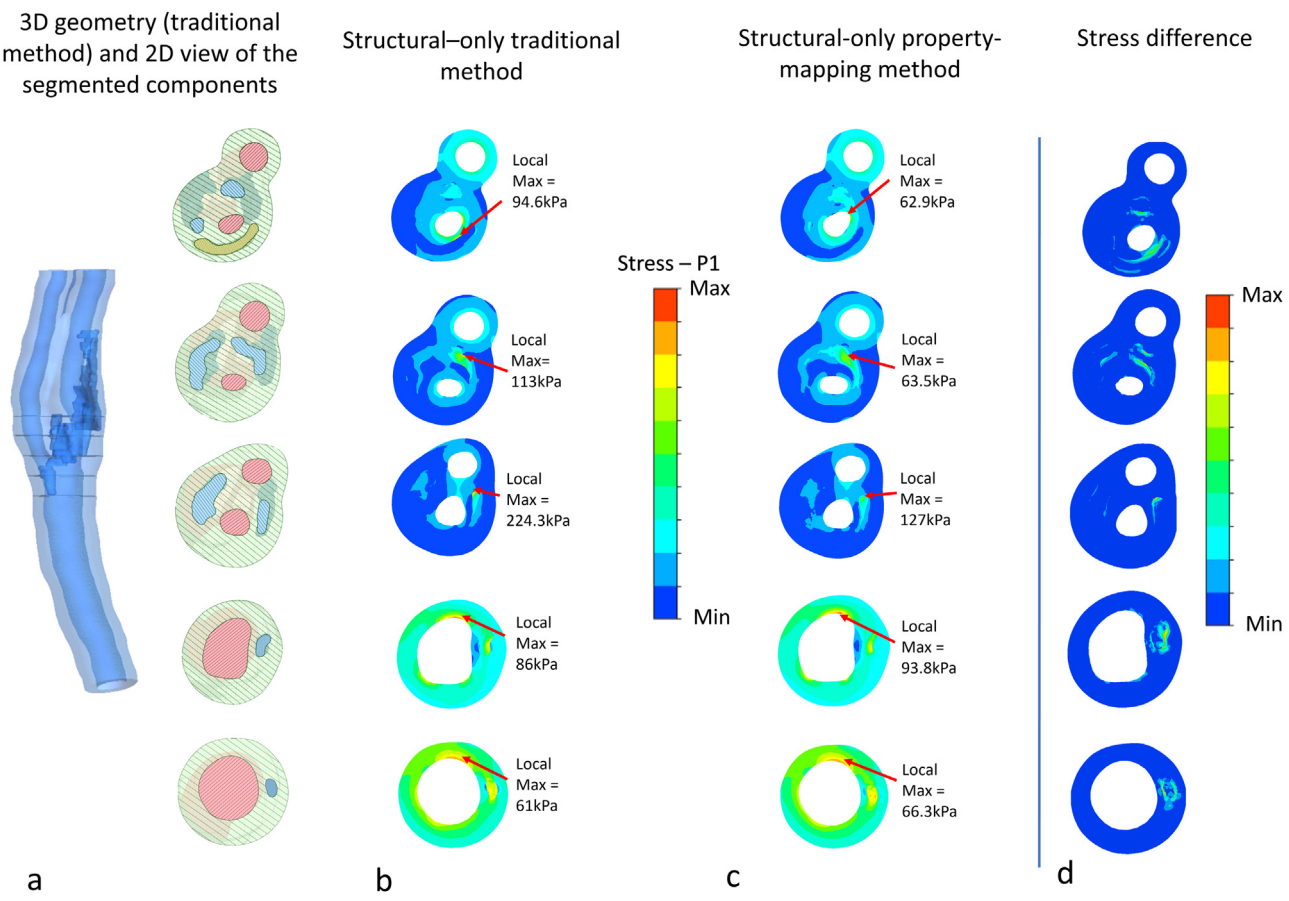

Fig. 5. Principal stress contours at five slices across the geometry from the 3D structural-only simulation. (a) 3D geometry used for the traditional method and the 2D views of the segmented components at the level of the selected slices (lipids=yellow, calcification=blue, arterial wall=clear yellow, and lumen=red), (b) Traditional method stress results, (c) Material-property-mapping stress results, and (d) stress difference between the two methods.

lipids identifiable in MRI. A characteristic slice was selected for the 2D structural analysis which contained both calcification and lipids as plaque components. To analyze the 3D structural-only and FSI, twenty-two slices were selected across the geometry. The average and maximum principal stress (Stress-P_1) values, as well as the location, were compared for the different slices. A subtraction between the stress contours from both methods was also performed to identify the approximate regions with the largest difference. Similarly, for WSS, the values from both methods were compared at systole and diastole. TAWSS and OSI were also computed to provide a more general observation through the cardiac cycle. TAWSS provides the overall WSS pattern and OSI characterizes the change in direction of the WSS vector from the main blood flow. As a verification method, the velocity contour at the level of the CCA from PC-MRI was compared to the velocity calculated by the FSI based on both methods. PC-MRI images were resampled to the same pixel dimension from which the geometries were reconstructed to compare the velocity contours. Also, the calculated mass flow rate at the outlets (ICA and ECA), in FSI simulations based on both methods were compared. All models were solved using ANSYS (version 19.0, ANSYS, Canonsburg, PA, USA).

3. Results

3.1. Stress comparison in 2D analysis

Figure 4 shows the information from the reconstruction of the labels using MRI to stress contours for both methods for a specific 2D geometry, as well as the material mapping result. The stress contours exhibit similar patterns between the two methods, with a slight decrease in stress from 150 kPa for the traditional method to 134 kPa for the mapping method. Notably, the location of maximum stress remains consistent across both methods.

3.2. Stress comparison in 3D structural-only analysis

The results of a 3D structural-only analysis comparing the traditional method and the mapping method are presented in Fig. 5. The figure displays five characteristic slices of the geometry and provides the principal stress contours and differences for both methods. While there is a difference in the maximum stress, the stress distributions are similar across both methods. In the first three slices, the mapping method resulted in a decreased maximum principal stress, with a maximum percentage difference of 40%, 56%, and 55%, respectively. In the last two slices, the maximum stress was located in the fibrous cap region and remained similar, with only an 8.6% and 8.31% difference. The greatest difference in stress values was observed at the interfaces between different plaque components and it was noticed that the location of the maximum stress changed in one of the analyzed slices.

3.3. Stress and WSS comparison in FSI analysis

Figure 6 shows the results of the principal stress difference from the structural component of the Fluid-Structure Interaction (FSI) simulations. Five intermediate slices, selected from those used in the 3D structural-only analysis, are presented. The maximum stress values calculated with the mapping method decreased in all

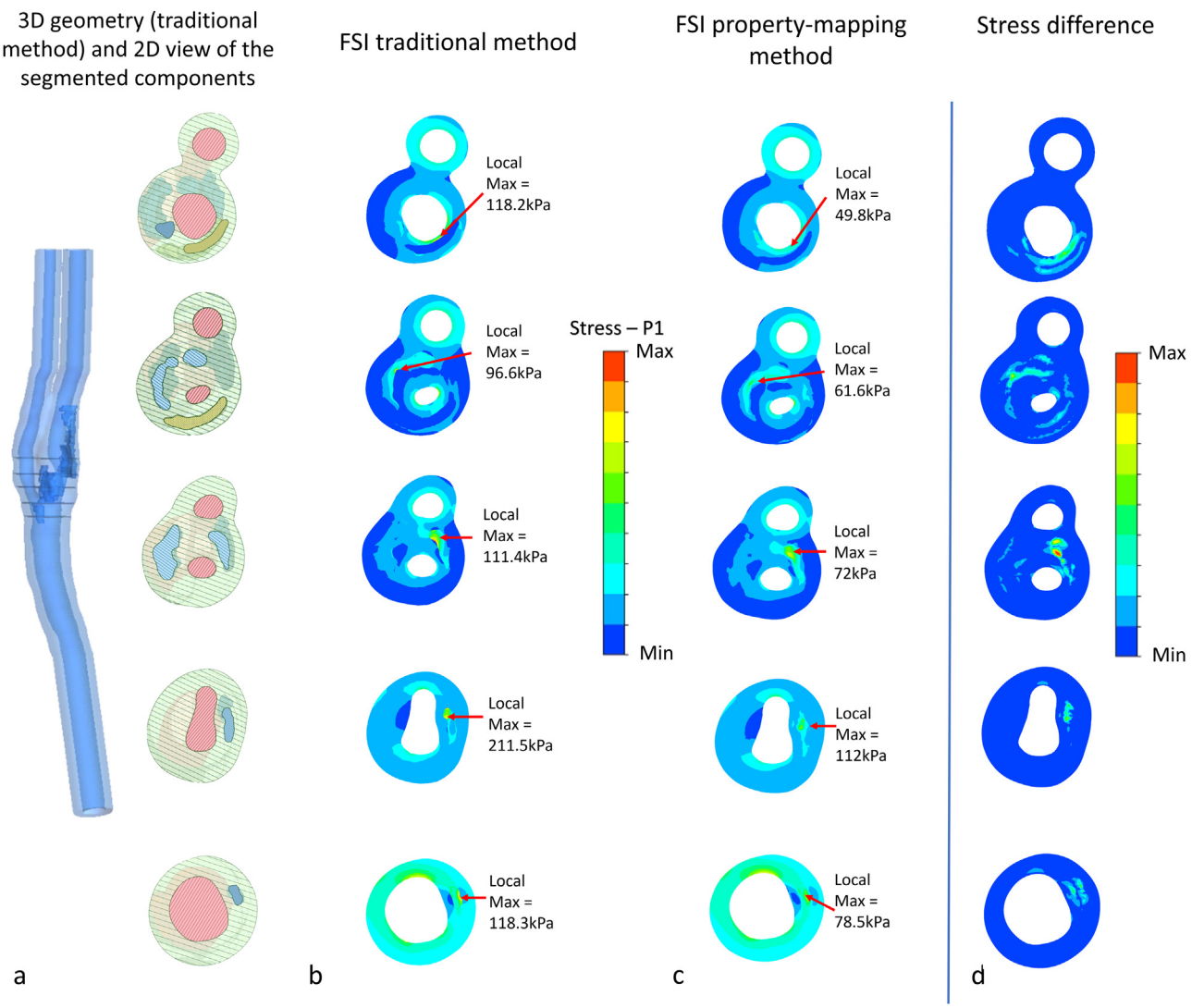

Fig. 6. Principal stress contours at five slices across the geometry from FSI simulation. (a) 3D geometry used for the traditional method and the 2D views of the segmented components at the level of the selected slices (lipids=yellow, calcification=blue, arterial wall=clear yellow, and lumen=red), (b) Traditional method stress results, (c) Material-property-mapping stress results, and (d) stress difference between the two methods.

slices, with a difference of 81%, 44%, 43%, 61.5%, and 40%, respectively. However, the stress distribution has a similar pattern and the locations of the maximum stresses are the same between the two methods.

Figure 7 illustrates the results in terms of Wall Shear Stress (WSS) contours for both methods and differences at systole and diastole. The WSS contours display identical patterns, with a maximum difference at systole and diastole of 20.5 and 2.2 Pa, respectively, located at the bulb after stenosis. The maximum WSS values calculated by the fluid component of the FSI, comparing both methods, tend to be similar with a difference of just 2.3 Pa at systole and 0.2 Pa at diastole. Time-averaged WSS (TAWSS) and Oscillatory Shear Index (OSI) have almost identical patterns and oscillatory regions, with just a 0.4 Pa maximum difference for TAWSS.

In the verification process, the velocity calculated from both methods exhibited the same patterns, as shown in Fig. 8. The maximum velocity calculated from the FSI in both methods remained the same and was lower by 10.5% compared to PC-MRI. Furthermore, the calculated mass flow rate at the internal carotid artery (ICA) and external carotid artery (ECA) for both methods was compared, as shown in Fig. 8(f). It can be observed that the calculated profile at the outlets (ICA and ECA) are similar, with a superposition across the cardiac cycle.

3.4. TAWSS and WSS comparison at systole and diastole from FSI

Additional analysis was conducted to examine the increase in maximum Wall Shear Stress (WSS), at systole and diastole, and Time-averaged WSS (TAWSS). The luminal area was calculated based on the location of the maximum WSS. It was discovered that the luminal area for the mapping method is slightly smaller in comparison to the traditional method, at systole and diastole (0.2% and 0.11% difference, respectively). This resulted in an increase in WSS due to the smaller luminal area. This is because the approach used to apply the material properties in each method also resulted in slightly different arterial deformation. The maximum stress was also slightly lower in the mapping method than in the traditional method, primarily due to the interpolation of material properties.

3.5. Maximum and average stress values

Figure 9 displays the results of the analysis performed for the maximum and average stress values, calculated at the 3D

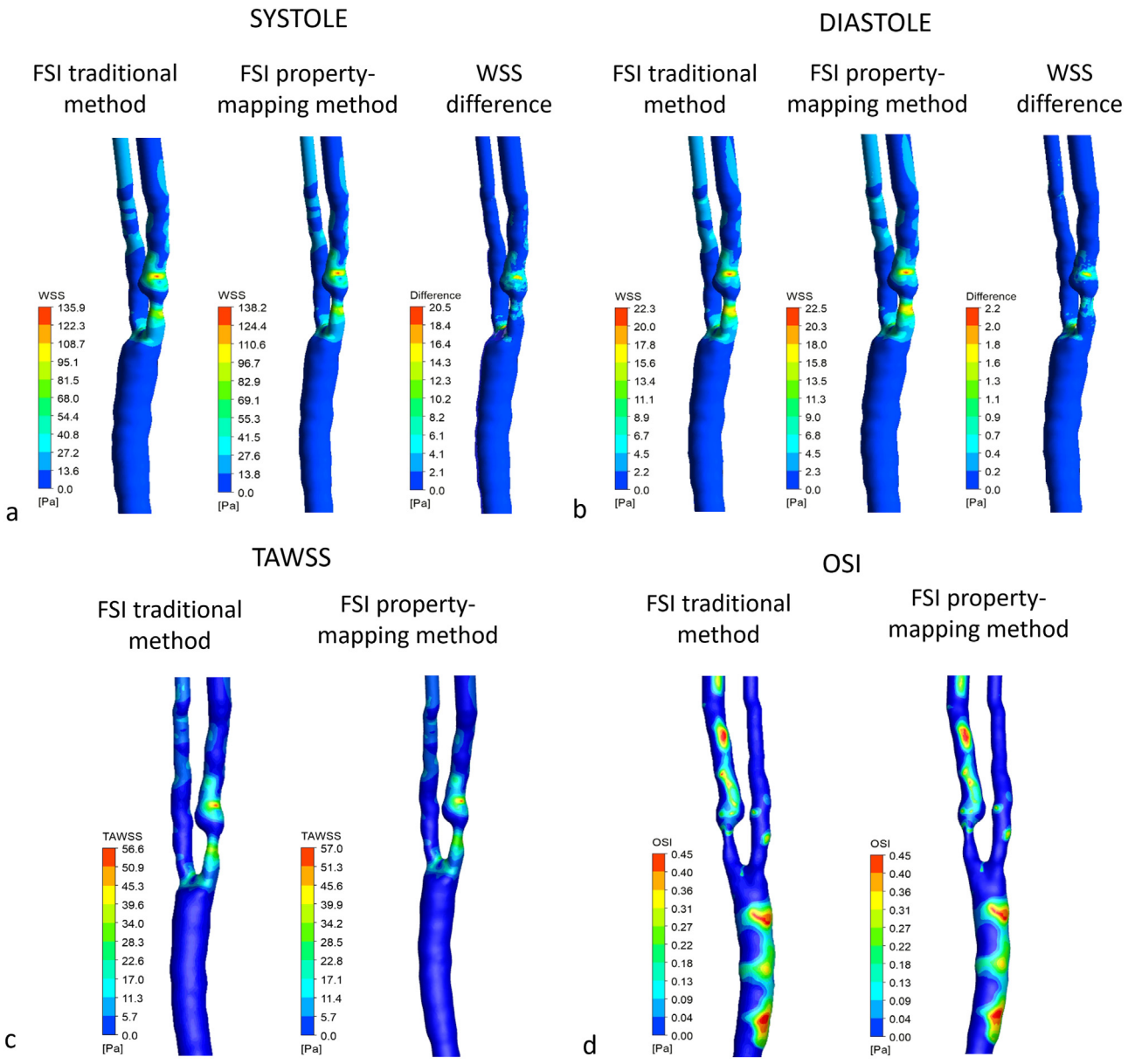

Fig. 7. WSS contours from the FSI calculation using the traditional, the material-property-mapping method, and the WSS difference between two methods at (a) systole and (b) diastole. As well as WSS descriptors (c) TAWSS and (d) OSI.

structural-only and the structural component of the Fluid-Structure Interaction (FSI) simulations, for 22 slices equidistantly distributed across the reconstructed plaque. The stresses calculated from the 3D structural-only and FSI simulations exhibit a similar pattern. The greatest differences were observed for the maximum stress values when comparing both methods in the presence of plaque components, as opposed to regions at the beginning and end of the plaque where the values remained similar. In terms of the average stress, the values tend to be consistent across the geometries for both methods.

4. Discussion

Figure 2 illustrates the reduction of mesh complexity from the traditional method to the mapping method. This is reflected in the ability to analyze structures that are closer to actual plaques, where the size of the components and their relation to the surrounding tissue is no longer a complex issue for meshing and, as a result, for structural simulation. In the traditional method, generating the mesh for complex geometries required an iterative process between reconstruction and meshing to achieve an acceptable and feasible mesh. In contrast, the mapping method resolves these issues by using a uniform mesh and assigning element-specific material properties, significantly reducing the total time from the 3D reconstruction to the calculation of results. Therefore, the advantage of the mapping method is that it eliminates the need for dedicated meshing in areas such as thin fibrous cap, contact, and interface regions, which often cause problems and require mesh updating in traditional Finite Element Analysis (FEA) to achieve a reasonable solution.

In terms of computation time and memory usage, the difference between the traditional and the mapping method is not significant. In certain instances, the mapping method may result in slightly longer computation time compared to the traditional method. However, the real advantage of the mapping method lies in the elimination of the often tedious and time-consuming pro-

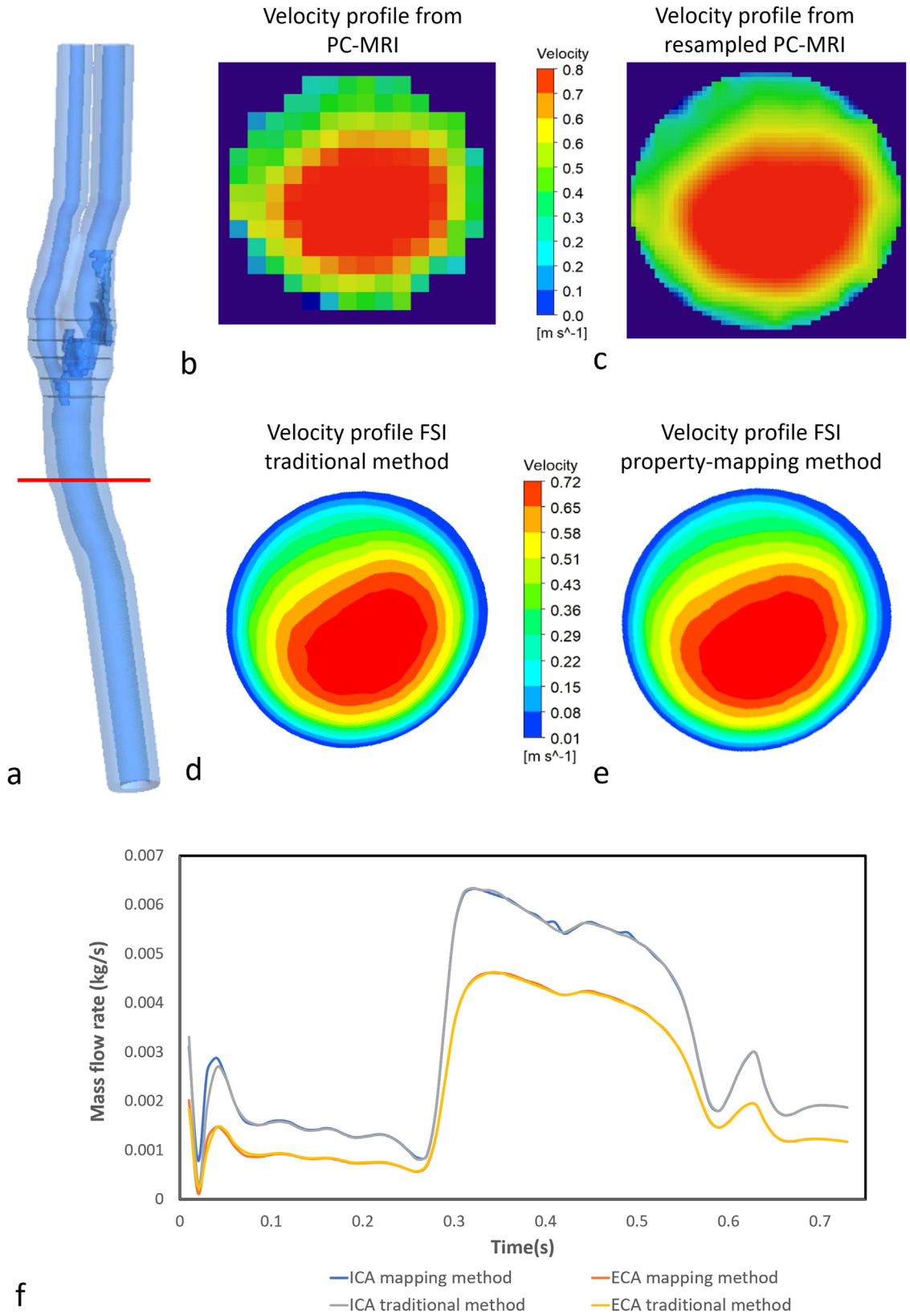

Fig. 8. Velocity profiles comparison at the level of CCA. (a) 3D carotid artery geometry and the red line shows the level at which the comparison was performed. The measured velocity contours from (b) PC-MRI, (c) resampled PC-MRI. The calculated velocity contours from FSI analysis using (d) the traditional method, and (e) the material-property-mapping method, (f) comparison between the calculated mass flow rate profiles at the ICA and ECA from both methods.

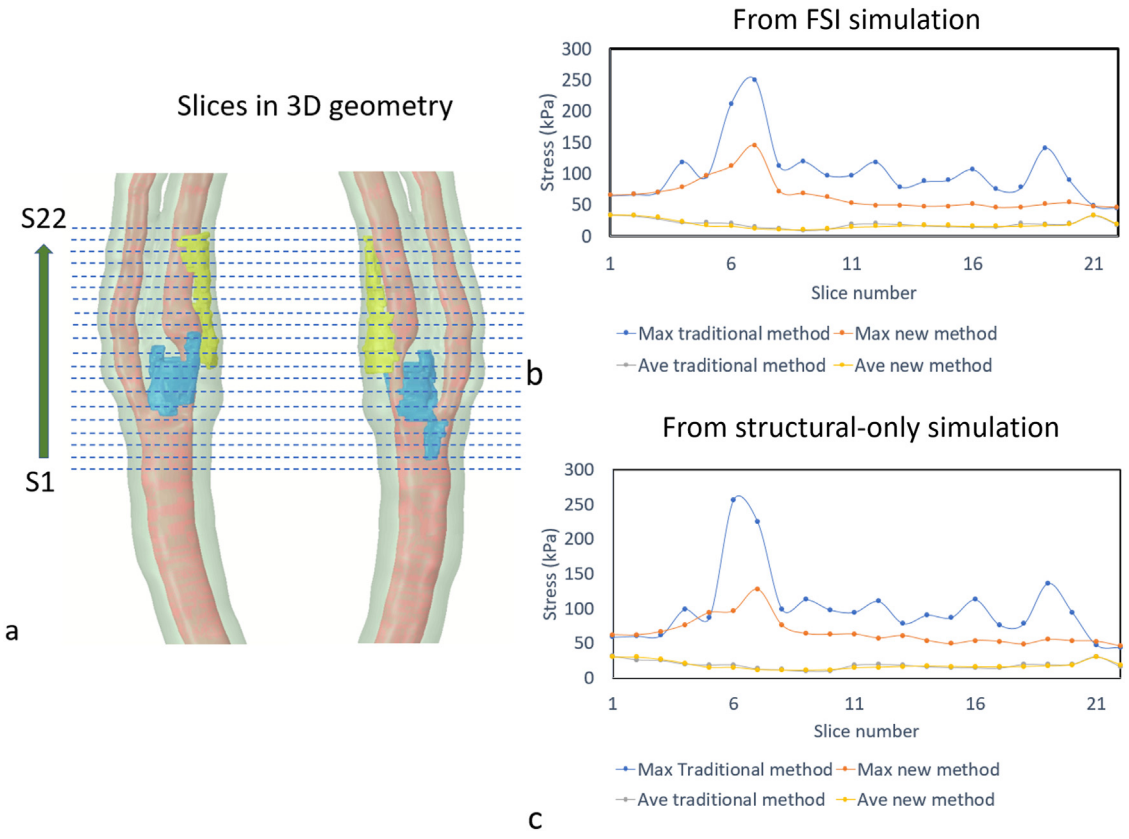

Fig. 9. Comparison of the maximum and average principal stresses between two methods. (a) Twenty slices across the carotid artery geometries (green=arterial wall, yellow=lipids, lumen=red, and calcification=blue), comparison of the (b) stress values calculated from FSI simulation, and (c) stress values calculated by the structural-only simulation.

cess of manually generating meshes for complex geometries and material distributions, which can take weeks depending on the complexity of the geometries.

The mapping method also allows for a certain level of transition between the material properties (Young's modulus) of the different components. In the traditional method, there is a sharp change between components, such as from calcification with 10 MPa to fibrous tissue of 0.6 MPa. This is the reason why the maximum stress values in the mapping method resulted in lower values compared to the traditional method, particularly in regions where calcification is present. Maximum stress values, however, tend to remain similar in situations where these values are located in the fibrous cap of the predefined slices. Peak stress values in structural analysis of plaque components have been widely associated with unstable and even possible ruptured plaques, particularly at the fibrous cap. Although the proposed method reduces the value of the maximum stresses (due to the elimination of sharp transitions between material properties), the location of the peak stress and the stress distribution tend to remain similar between the two methods. As expected, the difference between the two methods is observed at thin caps and interfaces between plaque components.

The mapping method allows for a transitional region mainly at the connection between tissues with large differences in material properties (Fig. 10). Therefore, histological analysis was performed on patient-specific atherosclerotic plaque tissue to further investigate the change in material properties. From Fig. 10(b) it can be observed that the main calcification section was removed by the cutting process, leaving behind at the edges, traces of calcification (depicted in dark purple). Similarly, Fig. 10(c) shows the transition between lipids and fibrous tissue from histological data (at 1X and 5X magnification). Figure 10(d, e, and f) also presents the distribution of Young's modulus of the plaque components and arterial wall using the mapping method. The highest interpolation range was in the transition from calcification to fibrous tissue (from 10 MPa to 0.6 MPa), which was approximately applied to two elements. But it was minimal in the transition from lipids to the arterial wall, due to the proximity of the material property values (0.02 MPa to 0.6 MPa). Fig. 10(e and f) provides a detailed view of the interpolation between different material properties using isolines and contours. Although the histological analysis provides an understanding of the material properties distribution in the patient-specific plaque tissue, further evaluations are required for tissue characterization to validate the proposed method.

As shown in Figs. 4, 5, and 6, the generated stress plots for 2D, 3D structural-only, and Fluid-Structure Interaction (FSI) simulations exhibit a high degree of consistency. This is further supported by the small differences between the calculated stress values in Figs. 5 and 6. Additionally, the Wall Shear Stress (WSS) and its descriptors calculated from the FSI simulations using both methods also show a high degree of agreement, as evidenced by the small differences between them. Further verification was performed using PC-MRI and the calculated velocity values from both methods, and it was observed that the maximum velocity values were tilted to one side due to the curvature of the geometry at this specific location, a pattern that was observed in the calculated results at the level of the CCA. Although the comparison was performed at the level of the CCA, an area with no presence of stenosis, changes in plaque characteristics downstream can affect the upstream flow. In this way, PC-MRI and WSS analysis provide another point of verification for the mapping method. The mass flow rate calculated at the outlets from both methods also served as a verification point and it was observed that both resulting profiles were similar.

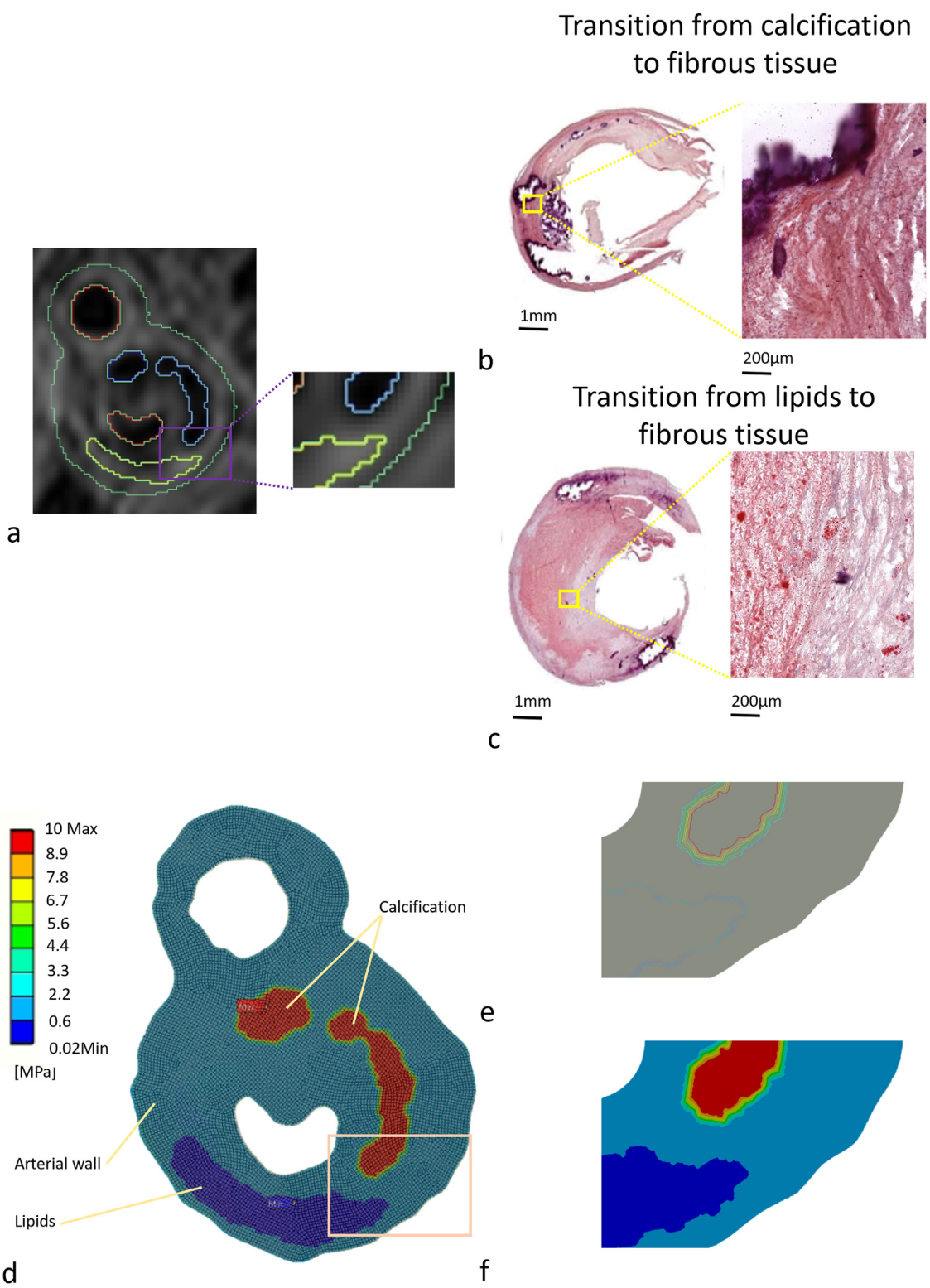

Fig. 10. (a) MRI images with labeled contours, and histological samples, highlighting the transition from (b) calcification to fibrous tissue, and (c) lipids to fibrous tissue. Analysis of the interpolation performed between the plaque components and the arterial wall by the material-property-mapping method showing, (d) Young's Modulus plot and mesh (lipids=0.02 MPa, calcification=10 MPa, and arterial wall=0.6 MPa), region of interest (e) illustrating the transition in between materials in isolines, and (f) final contours.

4.1. Limitations

4.1.1. Boundary conditions

The results of the numerical simulations are based on the geometry of the model, the loads or boundary conditions employed, and the material properties. In this study, the geometry and mass flow rate, prescribed at the inlet, are patient-specific; however, the material properties are still based on previous studies [14,20], where a linear elastic behavior was assumed for the arterial tissue, calcification, and lipids. Further investigation is required to apply

non-linear elastic material properties to the plaque components using the mapping method.

Also, at the outlets of the geometry, in the FSI simulation, the pressure was scaled up based on the mass flow rate profile and the arm pressure of the patient. This setup was adopted due to the complexity/impossibility of obtaining a realistic pressure profile at the carotid artery for each patient. Also, previous studies [21,22] have shown that the out-phase relationship between velocity and pressure is not remarkable as in other regions of the circulatory system such as the coronary artery. Therefore combining patient-specific arm pressure and the mass flow rate profile extracted directly from phase-contrast magnetic resonance imaging (PCMRI) provides a level of confidence.

4.1.2. Geometry shrinkage analysis

Another limitation of this study is that the shrinkage or zero-state pressure procedure was not performed in the geometries. More than 20 years ago, Fung [23] and Vaishnav and Vossoughi [24] independently demonstrated that the zero-stress state of a blood vessel is a crucial and unresolved issue. This seminal observation shifted our understanding from the previously assumed no-load configuration to the zero-stress state as the basis for blood vessel mechanics. Some studies have performed it using circumferential shrink and axial stretch ratio [25,26] in computational biomechanics of blood vessels. However, developing and validating a realistic shrinkage approach remains a challenge. In a previous study, the authors conducted a pre-shrinkage analysis on carotid arteries, using the residual stress calculated in the diastolic point of the cardiac cycle in a fluid-structure interaction (FSI) simulation [12]. This analysis revealed that P1-stress contours and maximum stresses remained similar.

While pre-shrinkage procedures are valuable, it is important to note that in this case, the two methods were compared under the same conditions. The current study aimed to propose a material properties mapping method and compare it to the traditional one, and considering shrinkage would not alter the main conclusion. Instead, it would increase computational expenditure and each plaque component may shrink differently, data that is not available.

4.1.3. Population

Future larger-scale patient studies are needed to further demonstrate the feasibility and advantage of the mapping method. It is also recognised that experimental validation can give further insight into the accuracy of both traditional and proposed methods.

5. Conclusion

A material property mapping method for stress analysis of atherosclerotic plaques was proposed in this study. The proposed method reduced the calculated maximum stress as compared to the traditional method while maintaining a similar stress distribution pattern. The feasibility and applicability of the mapping method in the numerical analysis of atherosclerotic plaques were demonstrated through its use in 2D, 3D structural-only, as well as 3D Fluid-Structure Interaction (FSI) simulations. Furthermore, it highlights the potential to simplify the generation of volume meshes for complex biological structures, such as carotid atherosclerotic plaques, using the proposed method, and pave the way for faster and more efficient patient-specific biomechanical analysis in the future.

Declaration of Competing Interest

The authors declare that they have no conflict of interest.

Acknowledgments

The authors would like to acknowledge the financial support from the Australian Research Council (DP200103492, DP200101970), National Nature Science Foundation of China (NSFC:11972118, 12172089, 61821002), the PA Research Foundation (PARF), and the Medical Research Future Fund (2016165). The authors would also like to thank the team at PA hospital, especially Gillian Jagger.

Supplementary materials

Supplementary material associated with this article can be found, in the online version, at doi:10.1016/j.cmpb.2023.107417.

References

[1] T. Leiner, S. Gerretsen, R. Botnar, E. Lutgens, V. Cappendijk, E. Kooi, J. van Engelshoven, Magnetic resonance imaging of atherosclerosis, Eur. Radiol. 15 (2005) 1087–1099, doi:10.1007/s00330-005-2646-8.
[2] J.F. Bentzon, F. Otsuka, R. Virmani, E. Falk, Mechanisms of plaque formation and rupture, Circ. Res. 114 (2014) 1852–1866, doi:10.1161/CIRCRESAHA.114.302721.
[3] S. Carr, A. Farb, W.H. Pearce, R. Virmani, J.S.T. Yao, H.S. Bassiouny, P. Gloviczki, Atherosclerotic plaque rupture in symptomatic carotid artery stenosis, J. Vasc. Surg. 23 (1996) 755–766, doi:10.1016/S0741-5214(96)70237-9.
[4] G.C. Cheng, H.M. Loree, R.D. Kamm, M.C. Fishbein, R.T. Lee, Distribution of circumferential stress in ruptured and stable atherosclerotic lesions: a structural analysis with histopathological correlation, Circulation 87 (1993) 1179–1187, doi:10.1161/01.CIR.87.4.1179.
[5] I. Division, M. Pharmacology, Biomechanics of Plaque rupture: progress, problems, and new frontiers, Ann. Biomed. Eng. 30 (2002) 524–536, doi:10.1114/1.1482781.
[6] Z.Y. Li, S. Howarth, T. Tang, M. Graves, J. U-King-Im, J.H. Gillard, Does calcium deposition play a role in the stability of atheroma? Location may be the key, Cerebrovasc. Dis. 24 (2007) 452–459, doi:10.1159/000108436.
[7] O.D. Drive, O.D. Drive, Effect of calcification modulus and geometry on stress in models of calcified atherosclerotic plaque, Cardiovasc. Eng. Technol. 5 (2014) 244–260, doi:10.1007/s13239-014-0186-6.
[8] U. Morbiducci, D. Gallo, M.A. Deriu, Outflow conditions for models of the carotid bifurcation : implications for indicators of abnormal flow, J. Biomech. Eng. 132 (2019) 1–11, doi:10.1115/1.4001886.
[9] U. Morbiducci, D. Gallo, D. Massai, R. Ponzini, M.A. Deriu, L. Antiga, A. Redaelli, F.M. Montevecchi, On the importance of blood rheology for bulk flow in hemodynamic models of the carotid bifurcation, J. Biomech. 44 (2011) 2427–2438, doi:10.1016/j.jbiomech.2011.06.028.
[10] J.B. Mendieta, D. Fontanarosa, J. Wang, P.K. Paritala, T. McGahan, T. Lloyd, Z. Li, The importance of blood rheology in patient-specific computational fluid dynamics simulation of stenotic carotid arteries, Biomech. Model. Mechanobiol. 19 (2020) 1477–1490, doi:10.1007/s10237-019-01282-7.
[11] J.R. Leach, V.L. Rayz, B. Soares, M. Wintermark, M.R.K. Mofrad, D. Saloner, Carotid atheroma rupture observed in vivo and FSI-predicted stress distribution based on pre-rupture imaging, Ann. Biomed. Eng. 38 (2010) 2748–2765, doi:10.1007/s10439-010-0004-8.
[12] J. Benitez, D. Fontanarosa, J. Wang, P.K. Paritala, T. McGahan, T. Lloyd, Z. Li, Evaluating the impact of calcification on plaque vulnerability from the aspect of mechanical interaction between blood flow and artery based on MRI, Ann. Biomed. Eng. (2020), doi:10.1007/s10439-020-02655-1.
[13] Q. Wang, G. Canton, J. Guo, X. Guo, T.S. Hatsukami, K.L. Billiar, C. Yuan, Z. Wu, D. Tang, MRI-based patient-specific human carotid atherosclerotic vessel material property variations in patients, vessel location and long-term follow up, PLoS ONE 12 (2017) 1–18, doi:10.1371/journal.pone.0180829.
[14] J. Wang, P.K. Paritala, J.B. Mendieta, Y. Komori, O.C. Raffel, Y. Gu, Z. Li, Optical coherence tomography-based patient-specific coronary artery reconstruction and fluid–structure interaction simulation, Biomech. Model. Mechanobiol. (2019), doi:10.1007/s10237-019-01191-9.
[15] H. Gao, Q. Long, M. Graves, J.H. Gillard, Z. Li, Carotid arterial plaque stress analysis using fluid – structure interactive simulation based on in-vivo magnetic resonance images of four patients, J. Biomech. 42 (2009) 1416–1423, doi:10.1016/j.jbiomech.2009.04.010.
[16] C. Yang, D. Tang, C. Yuan, T.S. Hatsukami, J. Zheng, P.K. Woodard, In Vivo/Ex Vivo MRI-based 3D non-Newtonian FSI models for human atherosclerotic plaques compared with fluid/wall-only models, Comput. Model. Eng. Sci. 19(3) (2007) 233–246.
[17] H. Gao, Q. Long, M. Graves, J.H. Gillard, Z.Y. Li, Study of reproducibility of human arterial plaque reconstruction and its effects on stress analysis based on multispectral in vivo magnetic resonance imaging, J. Magn. Reson. Imaging. 30 (2009) 85–93, doi:10.1002/jmri.21799.
[18] G. Finet, J. Ohayon, G. Rioufol, Biomechanical interaction between cap thickness, lipid core composition and blood pressure in vulnerable coronary plaque: impact on stability or instability, Coron. Artery Dis. 15 (2004) 13–20, doi:10.1097/00019501-200402000-00003.

[19] G.A. Holzapfel, G. Sommer, P. Regitnig, Anisotropic mechanical properties of tissue components in human atherosclerotic plaques, J. Biomech. Eng. 126 (2004) 657–665, doi:10.1115/1.1800557.
[20] P.K. Paritala, P.K.D.V. Yarlagadda, J. Wang, Y.T. Gu, Z. Li, Numerical investigation of atherosclerotic plaque rupture using optical coherence tomography imaging and XFEM, Eng. Fract. Mech. 204 (2018) 531–541, doi:10.1016/j.engfracmech.2018.11.002.
[21] A. Zambanini, S.L. Cunningham, K.H. Parker, A.W. Khir, S.A.M.G. Thom, A.D. Hughes, Wave-energy patterns in carotid, brachial, and radial arteries: a noninvasive approach using wave-intensity analysis, Am. J. Physiol. - Hear. Circ. Physiol. 289 (2005) 270–276, doi:10.1152/ajpheart.00636.2003.
[22] C.J. Broyd, J.E. Davies, J.E. Escaned, A. Hughes, K. Parker, Wave intensity analysis and its application to the coronary circulation, Glob. Cardiol. Sci. Pract. (2017) 2017, doi:10.21542/gcsp.2017.5.
[23] Y.F. SQLIU, Changes of zero-stress state of rat pulmonary arteries in hypoxic hypertension, J. Appl. Physiol. 70 (2023).
[24] R.N. Vaishnav, J. Vossoughi, Estimation of residual strains in aortic segments, in: C.W. Hall (Ed.), Biomed. Eng. II, 1983, pp. 330–333, doi:10.1016/B978-0-08-030145-7.50078-7. Pergamon.
[25] D. Tang, C. Yang, S. Huang, V. Mani, J. Zheng, P.K. Woodard, P. Robson, Z. Teng, M. Dweck, Z.A. Fayad, Cap inflammation leads to higher plaque cap strain and lower cap stress : an MRI-PET /CT-based FSI modeling approach, J. Biomech. 50 (2017) 121–129, doi:10.1016/j.jbiomech.2016.11.011.
[26] X. Huang, C. Yang, C. Yuan, F. Liu, G. Canton, J. Zheng, P.K. Woodard, G.A. Sicard, D. Tang, Patient-specific artery shrinkage and 3D zero-stress state in multi–component 3D FSI models for carotid atherosclerotic plaques based on in vivo MRI data, MCB Mol. Cell. Biomech. 6 (2009) 121–134.